Dalton Transactions

Accepted Manuscript

ROYAL SOCIETY OF CHEMISTRY

www.rsc.org/dalton

Journal Name

ARTICLE

Synthesis, luminescence, and anti-tumor properties of $MgSiO_3$:Eu-DOX-DPP-RGD hollow microspheres

Received 00th January 20xx,
Accepted 00th January 20xx

DOI: 10.1039/x0xx00000x

www.rsc.org/

Ruichan Lv,[a] Chongna Zhong, [a] Arif Gulzar, [a] Shili Gai, [a] Fei He, [a] Rui Gu,[b,]* Shenghuan Zhang, [a] Guixin Yang, [a] and Piaoping Yang[a,]*

In this report, $MgSiO_3$:Eu-DOX-DPP-RGD hollow microspheres employed for simultaneous imaging and anti-cancer therapy has been designed by sequentially loading anti-tumor drugs of doxorubicin (DOX), light-activated platinum(IV) pro-drug of PPD, and targeted peptide of NH_2-Gly-Arg-Gly-Asp-Ser (RGD) on $MgSiO_3$:Eu mesoporous hollow spheres, which was synthesized using solid SiO_2 spheres as sacrificed template by facile hydrothermal process based on the Kirkendall effect. The photoluminescence intensity of $MgSiO_3$:Eu has been optimized, which can emit recognized red signal *in vitro* and *in vivo* under modest ultraviolet (UV) irradiation. It was found that the platform has high biocompatibility and could be intracellular through fast and effective endocytosis with the aid of targeted peptide of RGD, and chemotherapeutic drugs of DOX and light-activated platinum(IV) pro-drug of DPP can be released from the carrier to induce obvious inhabitation effect to HeLa cancer cells (only survival rate of 17.4%), which has been verified by *in vitro* and *in vivo* results. Moreover, the *in vitro* result of photosensitizer ZnPc loaded carrier shows the system is not suitable for ZnPc induced photodynamic therapy. The apparent imaging effect and high anti-tumor efficacy of this functional system make it highly potential in actual clinical applications.

Introduction

Nowadays, as one of the most important anti-cancer therapeutic methods, chemotherapy has proceeded with great improvement to extend patients' lives and relieve their pain.[1] Still, the therapeutic efficiency is expected to be enhanced because of unspecific chemo-effect and multi-drug resistance after long-time administration.[2–5] Thus, drug delivery systems (DDSs) as nanomedicine technologies are proposed to improve anti-cancer efficiency intensively. Mesoporous silica-based materials have attracted considerable attention in DDSs due to the significant advantages including high physicochemical stability, good biodegradability and easy functionalization. Simultaneously, they could provide high storage capacity and exhibit sustained drug release kinetics.[6–12] Moreover, hollow-structure materials with spherical shape are favorable for drug delivery because of their injectable and ingestible properties with high surface area, tunable pore channels and volumes, and large hollow cavities which could store more drug molecules.[13–18]

Manipulable luminescent materials as a unique approach for visualizing morphological details in tissues and cells with subcellular resolution are increasingly used for highly contrasted and real-time bio-applications including drug and gene delivery and bio-sensing.[19–22] Conventional luminescent organic dyes are the most widely employed bio-probes with high quantum efficiency and high sensitivity which can realize single molecular detection, yet it is difficult to distinguish different probes because of narrow and un-modifiable excitation spectra.[23,24] Quantum dots with high photo-stability, high quantum yield, broad excitation spectra and narrow emission band are excellent fluorophores, but the high toxicity limits their applications *in vivo*.[25,26] Lanthanide doped crystals and complexes have attracted great attention owing to their excellent luminescent properties with various excitation wavelength based on their particular 4f–5d and 4f–4f electronic transitions, which can generate narrow and intense emission peaks.[27–34] Moreover, they own good photochemical/ physical stability and low toxicity.

To solve the leaking problem of dye fundamentally, it is meaningful but still a challenge to research about the comprehensive luminescence materials with functional structure. Especially, time-resolved luminescence imaging technique could typically utilize the long-life phosphorescence (up to millisecond), which is an effective strategy to completely eliminate the interference caused by auto-fluorescence and scattered light from tissue and cells.[35–38] To

a. Key Laboratory of Superlight Materials and Surface Technology, Ministry of Education, College of Material Sciences and Chemical Engineering, Harbin Engineering University, Harbin, 150001, P. R. China,Address here. Email: yangpiaoping@hrbeu.edu.cn

b. Department of Orthopedics, China-Japan Union Hospital of Jilin University, Changchun, 130033, P. R. China Email: ccgurui@hotmail.com

Electronic Supplementary Information (ESI) available: spectra of the samples under the excitation at 265 nm; the absorbance spectra of the supernatants and the loading amount and efficiency versus the DOX amount; FT-IR spectra of the samples; FT-IR spectrum of light-activated DPP; the release efficiency of Pt from DCMPs-DPP with different pH values of 5.5 and 7.0; the release efficiency with and without UV light irradiation; the postulated drug release pathway of DPP to Pt(II) drug. See DOI: 10.1039/x0xx00000x

date, several lanthanide ions, such as Eu^{3+}, Ce^{3+}/Tb^{3+}, Dy^{3+}, Sm^{3+} ions were doped to produce photoluminescence, and the most widely used visualization tools as the bio-probes in biomedical applications were Eu^{3+} and Ce^{3+}/Tb^{3+} ions.[39–49] Recently, we fabricated Ce^{3+}/Tb^{3+} doped lanthanum phosphate compound as anti-cancer drug carrier.[50] However, the short luminescent wavelength (500-600 nm) is easily scattered for the clinical detection.[51,52] From this consideration, new europium-doped materials with longer emission wavelength (600-700 nm) as potential luminescence-guided theranostic agent is desirable.

In this contribution, $MgSiO_3$:Eu-DOX-DPP-RGD for simultaneous imaging and anti-cancer therapy has been fabricated. Hollow mesoporous $MgSiO_3$:Eu was obtained using spherical solid silica as sacrificed template arising from Kirkendall effect. The photoluminescence emissions of $MgSiO_3$:Eu with different Eu^{3+} ions concentrations were investigated to obtain the optimized $MgSiO_3$:Eu down-conversion microparticles (DCMPs) as the final drug carrier. Dual anti-tumor drugs such as photodynamic agent (ZnPc), chemotherapeutics drug (DOX), photo-activated platinum(IV) pro-drug (DPP) were loaded and the cytotoxicity was detected, which indicate DOX and DPP drugs should be chosen for chemo-therapy instead of ZnPc for photodynamic therapy. The bio-compatibility and anti-cancer therapeutic efficacy of $MgSiO_3$:Eu-DOX-DPP-RGD were evaluated using MTT assay, and animal experiment *in vivo* and *in vitro* in detail.

Experimental section

Reagents and materials. All the chemical reagents in this experiment were used without further purification and of analytical grade, including Eu_2O_3 (from Sinopharm Chemical Reagent Co., Ltd.), tetraethoxysilane (TEOS), ammonium chloride (NH_4Cl), magnesium chloride ($MgCl_2$), phosphate buffered saline (PBS), glutaraldehyde (from Tianjin Kermel Chemical Co., Ltd.), aminopropyltrimethoxysilane (APTS), 1-(3-dimethylaminopropyl)-3-ethylcarbodiimide hydrochloride (EDC), Nhydroxysuccinimide (NHS), 3-4,5-dimethylthiazol-2-yl-2,5-diphenyl tetrazolium bromide (MTT), 4',6-diamidino-2-phenylindole (DAPI), zinc(II)-phthalocyanine (ZnPc), Doxorubicin (DOX), calcein AM, propidium iodide (PI), trypan blue (from Sigma-Aldrich Co. Ltd). Peptide NH_2-Gly-Arg-Gly-Asp-Ser (denoted as RGD) was synthesized by Sangon Biotechnology Co. Ltd (Shanghai, P. R. China).

Synthesis of solid SiO_2 spheres. Silica spheres with an average size of 190 nm were prepared using the Stöber sol-gel method. Typically, 50 mL of deionized water, 280 mL of ethanol, and 28 mL of ammonia water were mixed with stirring fiercely, and then 14 mL of TEOS were added drop by drop. After further reaction for 6 h, the precipitate was centrifuged and washed with ethanol for three times.

Synthesis of hollow $MgSiO_3$:Eu microspheres. 0.01 M $EuCl_3$ was firstly prepared by dissolving 0.352 g Eu_2O_3 into HCl with gradually heating, and dissolved into 100 mL deionized water for further use. $MgSiO_3$:Eu hollow spheres were prepared by a sacrificed template process using as-prepared colloidal silica as the sacrificed template. In a typical process for the synthesis of $MgSiO_3$:5%Eu, 0.7125 mmol of $MgCl_2$ and 2.5 mL (0.025 mmol) of 0.01 M $EuCl_3$ were added into 30 mL of deionized water with ultra-sonication, and then the precursor of SiO_2 (0.1 g) were added. After the solution was uniform, the mixture was transferred and sealed into an autoclave (50 mL). The $MgSiO_3$:5%Eu sample was generated after hydrothermal reaction at 140 °C for 12 h and washed with water and ethanol by centrifugation. After further drying in the air at 60 °C for 12 h, $MgSiO_3$:5%Eu hollow spheres were obtained. $MgSiO_3$:x%Eu hollow spheres with other concentrations (x = 0.5%, 1%, 2%, and 10%) of Eu^{3+} ions were synthesized by the similar process except for adjusting the amounts of $EuCl_3$.

Loading of different drug molecules. Before drug loading process, $MgSiO_3$:Eu was modified with APTS. 100 mg of $MgSiO_3$:Eu DCMPs were mixed with 1 mL of APTS (1:100 dissolved in deionized water). After stirred for 4 h at room temperature, the $MgSiO_3$:Eu-NH_2 precipitate was obtained by centrifugation with deionized water for several times to remove the free APTS molecules.

30 mg of $MgSiO_3$:Eu-NH_2 were added into 20 mL of water, 1 mL of EDC (6 mg mL^{-1}), 1 mL of NHS (2 mg mL^{-1}), and 20 mL of ZnPc (0.5 mg mL^{-1} with ethanol) were added and stirred continuously at room temperature in the dark. After stirred for 12 h, the mixture was washed with ethanol and deionized water for three times to remove free ZnPc. The blue precipitate ($MgSiO_3$:Eu-ZnPc) was obtained after drying in air at 60 °C for 12 h.

In a DOX loading process, 30 mg of $MgSiO_3$:Eu DCMPs were added into 20 mL of PBS and ultrasonically dispersed. Then, DOX (2.5 mg) was added into the solution and stirred for 12 h in the dark. The red precipitates ($MgSiO_3$:Eu-DOX) were separated by centrifugation and washed several times with deionized water. The supernatant was collected for UV-vis measurement to calculate the loading and release amount of DOX.

The synthesis of dicarboxyl light-activated platinum(IV) pro-drug of DPP was similar to the our previous literature.[53] Briefly, 30 mg of $MgSiO_3$:Eu-DOX DCMPs were dispersed into 20 mL of deionized water under ultrasonication. Then, 1 mL of EDC (6 mg mL^{-1}), 1 mL of NHS (2 mg mL^{-1}), and 3 mg of DPP were added into the above solution and stirred for 24 h away from light. After that, the red/yellow powders ($MgSiO_3$:Eu-DOX-DPP) were obtained. The supernatant was recovered for further ICP-MS measurement to evaluate the loading and release amount of DPP.

Modification of RGD peptide. Typically, 10 mg of DCMPs-drug was covered by 5 mL of solution with concentration of 1 mg mL^{-1} RGD peptide in PBS. Meanwhile, 1 mL of EDC (6 mg mL^{-1}), 1 mL of NHS (2 mg mL^{-1}), and 5 mL of PEG-NH_2 (10 mg mL^{-1}) were also added for better chemical conjunction and bio-compatibility. After stirred for 4 h at room temperature, DCMPs-drugs-RGD was obtained.

Characterization. Powder X-ray diffraction (XRD) measurement was performed on a Rigaku D/max TTR-III diffractometer using Cu Kα radiation (λ = 0.15405 nm) with scanning rate of 15°/min in the 2θ range of 20°-80°. The

morphology and structure were recorded on scanning electron microscope (SEM, JSM-6480A), transmission electron microscopy (TEM, FEI Tecnai G^2 S-Twin). N_2 adsorption/ desorption isotherms were recorded on a Micromeritics ASAP Tristar II 3020 instrument, and the pore size distribution was determined through Barrete-Jonere-Halenda (BJH) method. Fourier transform infrared spectroscopy (FT-IR) spectra were obtained on a Perkin-Elmer 580B IR spectrophotometer using the KBr pellet as the background. DC emission spectra were measured in the UV regions (200-400 nm) and visible regions (400-800 nm) using xenon lamp as the irradiation source on an Edinburgh FLS 980 instrument. DOX concentration was detected by UV-1601 spectrophotometer. Confocal laser scanning microscopy (CLSM) images were recorded using Leica TCS SP8. Inductively coupled plasma (ICP) was carried out on a Thermo Electron X Series II ICP instrument.

***In Vitro* bio-compatibility using MTT assay.** Standard MTT assay was carried out using L929 cell lines. Firstly, L929 cells were put in a 96-well plate (about 6000 per well) to obtain monolayer, and then material was added with gradient concentrations (1000, 500, 250, 125, 62.5, 31.3, and 15.6 μg mL^{-1}). As the control group, the blank was added with pure culture. After incubated for another 24 h, 20 μL of MTT solution was added to each well, and incubated for another 4 h. Then, the mixture was discarded, and DMSO (150 μL) solvent was added to dissolve the produced formazan. Finally, the plate was put on the micro-plate reader, and the absorbance values were recorded at the wavelength of 490 nm.

Hemolysis assay. Typically, human red blood cells (RBCs) were centrifugated and washed with PBS five times to remove the serum. Then, the RBCs were diluted with PBS (1:10). After that, 0.4 mL of diluted RBCs solution was mixed with 1.4 mL of PBS (as a negative control), 1.4 mL of deionized water (as a positive control), and 1.4 mL of materials with different concentrations of 1000, 500, 250, 125, 62.5, and 31.3 μg mL^{-1}, respectively. The eight samples were shaken and kept for 2 h. After that, the solutions were centrifuged and the absorbance of the upper supernatants was measured on the micro-plate reader (at the wavelength of 450 nm). The hemolysis percentage was calculated as: Hemolysis (%) = (A_{sample} - $A_{control(-)}$) / ($A_{control(+)}$ - $A_{control(-)}$), where A is the absorbance.

***In vitro* cellular uptake.** Typically, HeLa cells were cultured in the 6-well plate together with coverslips to obtain monolayer cells. Then, 1 mg mL^{-1} of DCMPs was added with incubation times of 30 min and 1 h at 37 °C, respectively. For the comparison of the RGD adhesion properties, DCMPs-RGD was incubated with cells for 10 min. After that, the cells were washed with PBS and fixed with 2.5% glutaraldehyde (1 mL $well^{-1}$) for 10 min. After further rinsed with PBS, the cells were stained with DAPI solution (5 μg mL^{-1} in PBS, 1 mL $well^{-1}$) for 10 min for nucleus labeling. Then, the coverslips were placed on a glass microscope slide after further being washed with PBS. The states of cells were recorded by Leica TCS SP8.

***In vitro* cytotoxicity using MTT assay.** Typically, HeLa cells were incubated in two 96-well plates to obtain monolayer cells, and then different materials were added. The concentration of drug carrier was 500, 250, 125, 62.5, 31.25, and 15.63 μg mL^{-1}, respectively. The corresponding drug concentration of ZnPc is 50, 25, 12.5, 6.25, 3.13, and 1.56 μg mL^{-1}, and the corresponding drug concentration of DOX is 34, 17, 8.5, 4.25, 2.13, and 1.06 μg mL^{-1}. After 24 h incubation with the different materials, the two plated are separate into two groups. In Group I, there are three different treatments: DCMPs with no treatment, pure ZnPc under 650 nm irradiation, and DCMPs-ZnPc-RGD with UV irradiation. In Group II, there are also three different treatments: pure DOX, DCMPs-DOX-RGD, DCMPs-DOX-DPP-RGD, and all the three groups were under modest UV irradiation (0.2 W cm^{-2}). Then, 20 μL of MTT solution was added to each well, and incubated at 37 °C with another 4 h. After that, the mixture was discarded with another 150 μL of DMSO solvent. Finally, the plates were put on the micro-plate reader, and the absorbance values were recorded at the wavelength of 450 nm.

***In vitro* cytotoxicity marked by AM and PI.** The experiment was carried out on HeLa cells markedly by calcein AM or PI. Typically, HeLa cells were incubated in 6-well plate to obtain a monolayer, and then HeLa cells were treated with different methods: with DCMPs for 60 min, with DCMPs–DOX-DPP-RGD for 60 min, with DCMPs–DOX-DPP-RGD under UV irradiation for 8 h. After irradiation, the cells were rinsed with PBS three times, and 2 mL of calcein AM/PI (1:1) were added and kept at 37 °C for another 30 min. Finally, the coverslips were washed with PBS and recorded by Leica TCS SP8 instrument.

***In vivo* anti-cancer efficacy.** Female Kunming mice (20–25 g) were purchased from Harbin Veterinary Research Institute, Chinese Academy of Agricultural Sciences (Harbin, China), and all the mouse experiments were performed in compliance with the criterions of The National Regulation of China for Care and Use of Laboratory Animals. The tumors were generated in the left axilla of each female mouse through injection of H22 cell lines subcutaneously. After grown for a next week, the tumor size is about 8-10 mm, the mice were randomly separated into three groups (each group has five mice) and injected intratumorally with nothing as control group, with pure DOX, with DCMPs-DOX-DPP-RGD under UV irradiation, respectively. The mouse was injected every three days with the amount of 100 μL (concentration of 1 mg mL^{-1}). The tumor site was irradiated by the laser for 30 min every time (pump power is 0.2 W cm^{-2}). The tumor sizes and body weights were detected and recorded every two days.

Histology examination. After treatments for one week, the tumor in the third group was separate and staining with hematoxylin and eosin (H&E) for pathology analysis. After final treatments for two weeks, the representative organs of heart, liver, spleen, lung, kidney in the control group and the third group are separated, and tumor sites in all the three groups are also taken and sliced. After dehydrated using buffered formalin, ethanol of different concentrations, and xylene, the dehydrated tissues were embedded and sliced for H&E staining.

Results and discussion

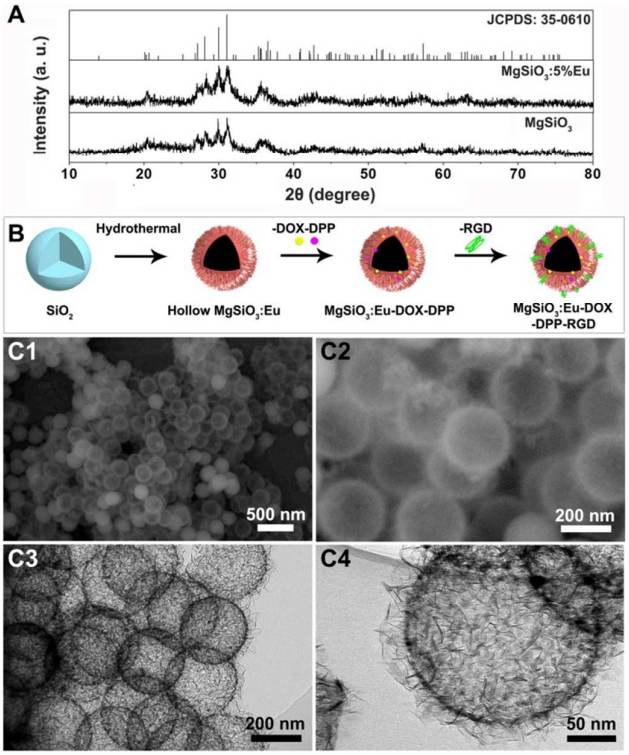

Fig. 1 (A) XRD patterns of $MgSiO_3$ and $MgSiO_3$:Eu. (B) Schematic diagram for the synthesis and modification of $MgSiO_3$:Eu DCMPs. (C1, C2) SEM images and (C3, C4) TEM images of hollow $MgSiO_3$:Eu DCMPs.

Phase, morphology, structure, and luminescent properties. As shown in Fig. 1A, by utilizing the silica as the sacrificed template under hydrothermal environment, the diffraction peaks of as-synthesized $MgSiO_3$ and $MgSiO_3$:5%Eu are both consistent with the monoclinic $MgSiO_3$ (JCPDS: 35-0610). This indicates the little amount of Eu^{3+} ions have no influence on the final phase of $MgSiO_3$. The actual molar concentrations of Eu^{3+} determined by the ICP-MS result are shown in Table S1, which are much similar to the stoichiometric ratios. The schematic illustration of the synthesis and modification with drug molecules on $MgSiO_3$:Eu DCMPs are presented in Fig. 1B. Hollow $MgSiO_3$ spheres are formed on the surface of sacrificed solid silica due to the Kirkendall effect. When SiO_2 precursor is under the hydrothermal environment, the core dissolves and the hollow shell forms *in situ* due to the different diffusion rates between the dissolution of cores and generation of the outer shell. In the SEM and TEM images (Fig. 1C1-C4), hollow $MgSiO_3$:Eu spheres show high dispersity with an average size of 230 nm.

N_2 adsorption/desorption isotherm of hollow $MgSiO_3$:Eu is given in Fig. 2A. It is clear that the as-synthesized $MgSiO_3$:Eu shows a typical IV-type isotherm with H1 hysteresis loop, indicating the typical mesoporous channel. The BET surface area, total pore volume, and average pore width are calculated to be 112 m^2/g, 0.267 cm^3/g, and 10.1 nm, respectively. The pore size distribution as shown in Fig. 2B indicates there is a main size focused on 3.49 nm which is attributed to the spinous shells.

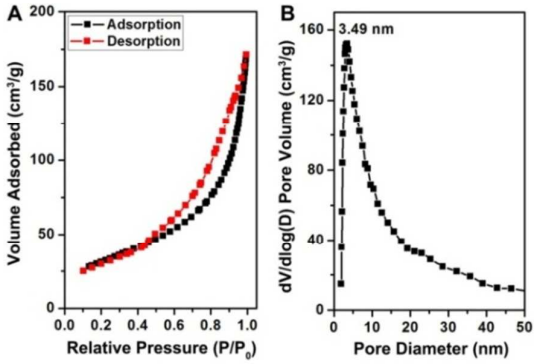

Fig. 2 (A) N_2 adsorption/desorption isotherm and (B) the pore size distribution of $MgSiO_3$:Eu DCMPs.

Fig. 3A-E shows the photoluminescence spectra of hollow $MgSiO_3$:x%Eu with different Eu^{3+} concentrations (x = 0.5%, 1%, 2%, 5%, and 10%) under the excitation at 265 nm. After comparing the excitation spectra of the sample holder and pure $MgSiO_3$ (Fig. S1) together with the reported literature,[54] we can infer that the broad peak at the wavelength of 365-395 nm is assigned to the f-f transitions of Eu^{3+} ions and the $MgSiO_3$ host. Also, the photographs of different $MgSiO_3$:x%Eu phosphors under 265 nm irradiation are shown in insets of Fig. 3A-E, they all emit bright red emissions even under daylight. $MgSiO_3$:5%Eu has the highest luminescence intensity, meaning the optimized concentration of Eu^{3+} ions is 5%. When the $MgSiO_3$:5%Eu is excited at the wavelength of 378 nm, the emission spectrum (Fig. 3F) consists of four peaks at 596, 615,

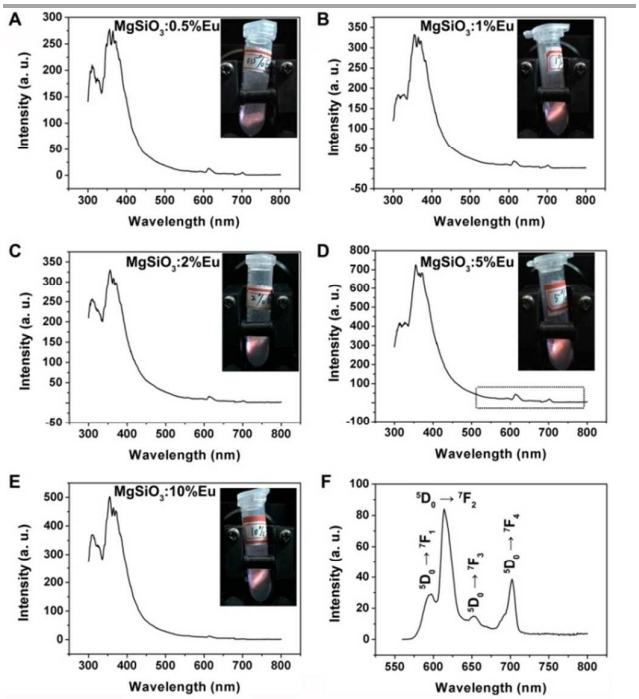

Fig. 3 DCL emission spectra of (A) $MgSiO_3$:0.5%Eu, (B) $MgSiO_3$:1%Eu, (C) $MgSiO_3$:2%Eu, (D) $MgSiO_3$:5%Eu (E) $MgSiO_3$:10%Eu excited at the wavelength of 265 nm. Insets are the corresponding photographs exposed under UV laser in daylight. (F) DCL emission spectrum of $MgSiO_3$:Eu excited at the wavelength of 378 nm.

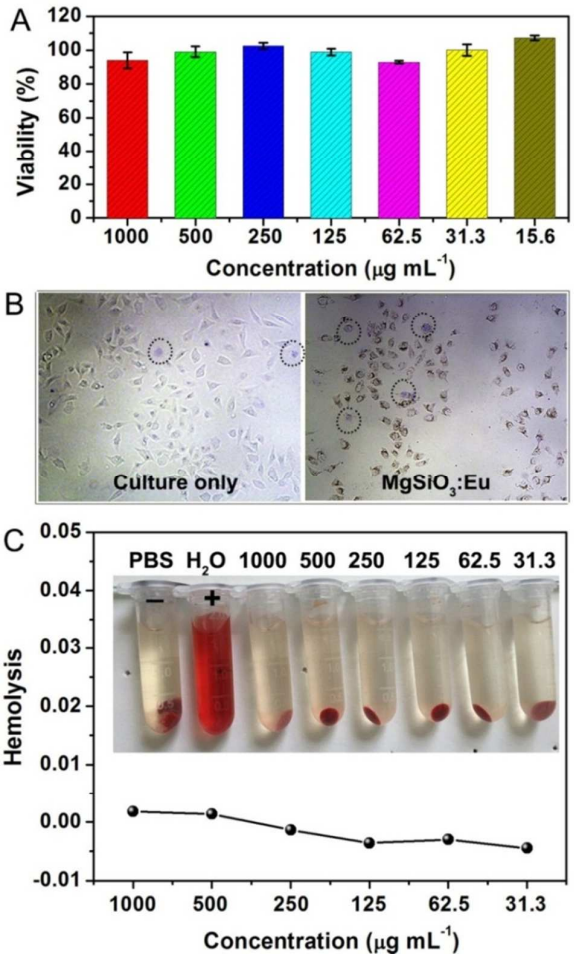

Fig. 4 (A) MTT assay using L929 cell lines incubated with $MgSiO_3$:Eu DCMPs with different concentration. (B) Optical microscopy images of L929 cells incubated with culture only and with $MgSiO_3$:Eu DCMPs for 24 h marked by trypan blue. (C) Hemolysis assay of $MgSiO_3$:Eu using human blood red cells.

669, and 702 nm, which are attributed to the $^5D_0 \rightarrow {}^7F_1$, $^5D_0 \rightarrow {}^7F_2$, $^5D_0 \rightarrow {}^7F_3$, and $^5D_0 \rightarrow {}^7F_4$, respectively.[55,56] This UV/vis excitation produced red luminescence emission can be potentially used for bio-imaging *in vitro* and *in vivo*.

Bio-compatibility, *in vitro* and *in vivo* anti-tumor properties. As the potential drug carrier used in DDSs, it is essential to evaluate the bio-compatibility of the material. Here, MTT assay using L929 cell lines incubated with hollow $MgSiO_3$:Eu spheres was carried out. As shown in Fig. 4A, the viabilities of L929 cells are up to 92.9%-107.2% after 24 h incubation with the material concentrations of 15.63 to 500 μg mL^{-1}. Even under the highest concentration of 1000 μg mL^{-1}, the viability is still as high as 94.0%. Additionally, the optical microscopy images of L929 cells incubated with culture only and with $MgSiO_3$:Eu spheres (both of the two samples concentrations are 1000 μg mL^{-1}) after 24 h marked by trypan blue are also presented in Fig. 4B. As depicted, there are few dead cells when incubated with $MgSiO_3$:Eu. For further clinical application, the hemolysis

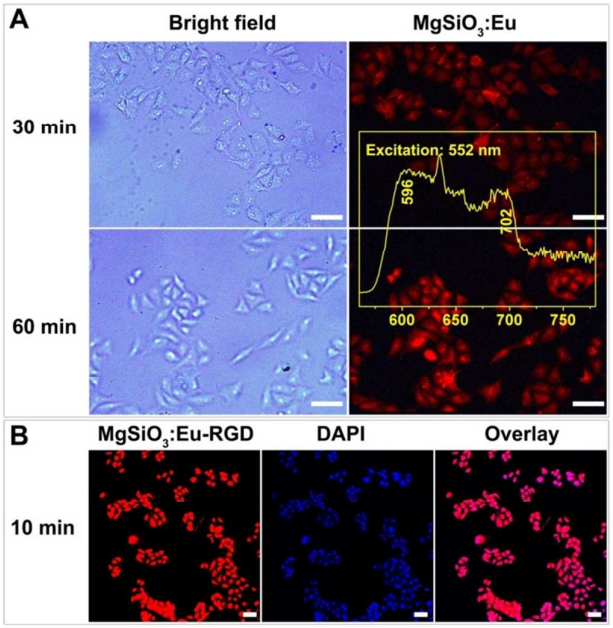

Fig. 5 (A) Optical microscopy and CLSM images of HeLa cells incubated with $MgSiO_3$:Eu DCMPs for uptaken times of 30 min and 60 min. (B) CLSM images of HeLa cells incubated with $MgSiO_3$:Eu-RGD for 10 min. All the scale bars are 50 μm.

property is essential to detect. As shown in Fig. 4C, the PBS solutions of RBCs with different concentrations of the material in the tubes have no obvious hemolysis. The highest hemolytic percentage of $MgSiO_3$ hollow spheres is only 0.18%. The results indicate the material is stable with RBCs. The MTT assay and hemolysis assay reveal that $MgSiO_3$:Eu DCMPs have good *in vitro* and *in vivo* bio-compatibility to normal cells.

The commonly used fluorescent dyes may confront the disadvantages of hydrophobicity and leaking as the imaging probes *in vitro*. Here, when as-synthesized $MgSiO_3$:Eu was utilized as drug carrier, the carrier itself could emit red luminescence through convert energy transfer process under the *in vitro* detection wavelength (552 nm). The spectrum of $MgSiO_3$:Eu excited at the wavelength of 552 nm is shown in inset of Fig. 5A, and there is still strong emission in 596-702 nm

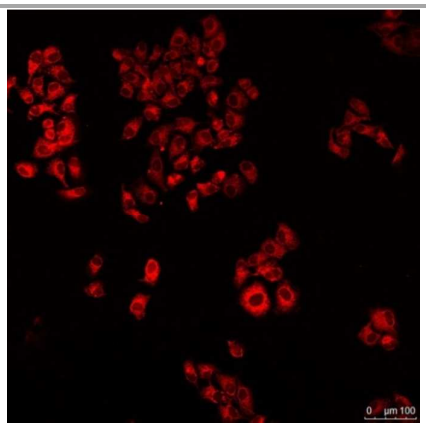

Fig. 6 CLSM image of HeLa cells incubated with $MgSiO_3$:Eu spheres for 30 min.

(red regions). It should be emphasized that there could be an obvious energy transfer process under the excitation of 552 nm. Meanwhile, there are stronger red signals with the enhanced incubation time from 30 min to 60 min in Fig. 5A. The CLSM image of HeLa cells incubated with $MgSiO_3$:Eu spheres for just 30 min are also shown in Fig. 6. It is obvious that the particles mainly locate in the cytoplasm, which further proves the spheres could be intracellular through the lysosome and endosome. Notably, when RGD is conjugated on the surface of $MgSiO_3$:Eu spheres, there is strong red signals even when the incubation time is as short as 10 min, which indicates $MgSiO_3$:Eu-RGD could be intracellular through fast and effective endocytosis.

Fig. 7A further presents the emission spectrum of $MgSiO_3$:Eu excited at the wavelength of 395 nm. Compared with the emission spectrum in Fig. 3 (with the excitation wavelength of 378 nm), the emission peaks are similar due to the energy transfer process of photons in the same energy levels. Fig. 7B shows the excitation spectrum with the emission wavelength of 615 nm, and there is several main excitation peaks at 259, 290 nm due to the Eu-O transitions, and 365, 378, 395 nm due to the f-f transitions and the host.[57] The result indicates the similar excitation wavelength or emission wavelength could be consistent with similar emission or excitation spectra, which contribute to the adjacent energy transfer processes. Furthermore, when the live/dead state of HeLa cells are used to evaluate the cytotoxicity of the drug loaded system, the excited wavelength using for CLSM is 488 nm. As shown in Fig. 7C, there are still red emissions (no matter the excitation wavelength is 265 nm, 395 nm, 488 nm, or 552 nm), which could be used for diagnosis. When $MgSiO_3$:Eu was incubated with HeLa cells for 60 min dyed with calcein AM, the CLSM image of HeLa cells (Fig. 7D) indicate that the cytoplasm of live cells present yellow instead of green color (due to pure calcein AM) because of the luminescent $MgSiO_3$:Eu itself.

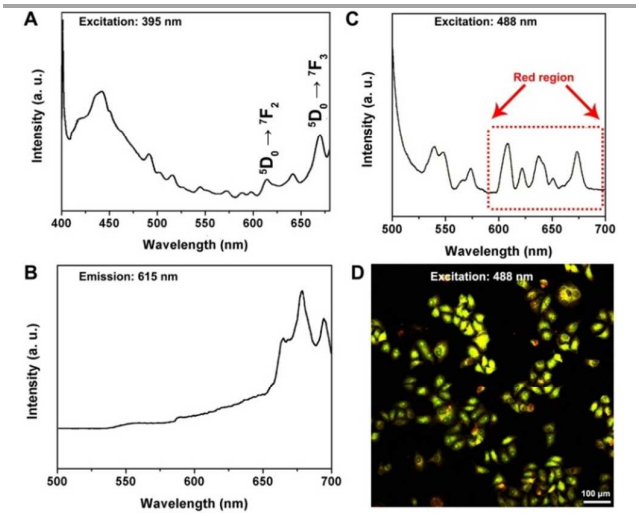

Fig. 7 (A) DCL emission spectrum of $MgSiO_3$:Eu excited at the wavelength of 395 nm. (B) Excitation spectrum with the emission wavelength of 615 nm. (C) DCL spectrum and (D) CLSM image of HeLa cells incubated with $MgSiO_3$:Eu for 60 min dyed with calcein AM/PI excited by the wavelength of 488 nm.

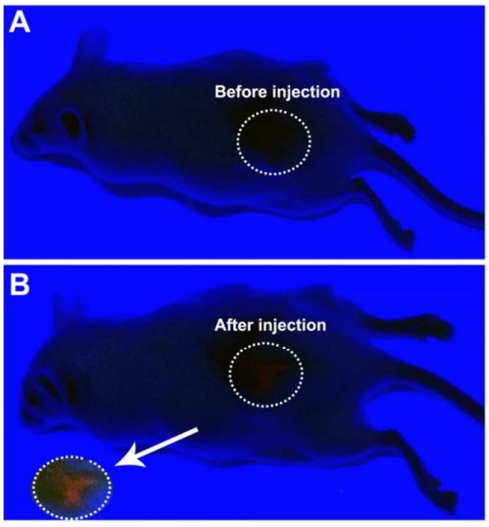

Fig. 8 Fluorescence photographs of a mouse (A) before and (B) after subcutaneous injection with $MgSiO_3$:Eu-DOX-DPP-RGD under UV irradiation (0.2 W/cm^2) in the dark room.

The fluorescence photographs of a mouse before and after subcutaneous injection with $MgSiO_3$:Eu under UV irradiation (0.2 W cm^{-2}) in a dark room are shown in Fig. 8. Due to the low pump power, the red emission seems not so bright yet could be recognized by naked eyes (as depicted in Fig. 3). Thus, it should be potential used in the DDSs for anti-cancer therapy because the clinical pump power could be much higher.

Here, three different drug models (photosensitizer of ZnPc, chemotherapy drugs of DOX and light-activated prodrug of DPP) were utilized to evaluate the anti-cancer therapeutic efficacy. As shown in Fig. 9A, the UV-vis absorbance spectrum of ZnPc solution indicates there is a strong absorbance in the red region which overlaps with the emission of $MgSiO_3$:Eu. In Fig. 9B, the final cytotoxicity to HeLa cells incubated with $MgSiO_3$:Eu with different concentrations has high viability of 86.2%-102.7%, indicating the material itself is low toxic to cancer cells. When pure ZnPc was added to the HeLa cells under 650 nm irradiation (pump power of 0.72 W cm^{-2}), the viability of cells is 46.2%-83.0%. However, when $MgSiO_3$:Eu-ZnPc was added under the UV irradiation (pump power of 0.2 W cm^{-2}), the viability is high as 54.1%-74.9%. The IC_{50} values of pure ZnPc and $MgSiO_3$:Eu-ZnPc with UV irradiation are 16.8 μg mL^{-1} and over 25 μg mL^{-1}, respectively. These data show the platform with loaded photosensitizer of ZnPc is failed to obtain a satisfactory anti-cancer therapeutic result. The reason should be that the UV irradiation has lower penetration and simultaneously the obtained red emissions could not stimulate ZnPc adequately to generate reactive oxygen species.

Then, we chose DOX and light-activated DPP as dual drugs. The UV-vis spectrum of DOX is presented in Fig. 9C, and there is a wide absorbance in 400-550 nm (blue and green region). The absorbance in this region has no side effect to the diagnosis in this platform, as they avoid the fluorescence quenching. As DOX (doxorubicin hydrochloride) can easily be dissolved into the water, hollow mesoporous structure and chemical conjunction (-NH_2) were utilized to enhance the

loading efficiency and remedy the leaching effect when they were used under the aqueous environment. The loading amount can be controlled by adjusting the added DOX amount. The absorbance spectra of the supernatants with different added amount are shown in Fig. S2A, and the corresponding curves of loading amount and loading efficiency *versus* the DOX amount are presented in Fig. S2B. It can be seen that the loading amount decreases while loading efficiency increases with the decreased added DOX amount (Table S2), which should be due to the saturation of molecules in the cavities and chemical bands. The final utilized DOX amount is 2.5 mg, which has the proper balance between the loading amount and efficiency simultaneously. The release efficiency curves in Fig. 9C indicate that DOX could be released with a fast beginning and slower release platform, and there is an evident difference between the acid (tumor cell microenvironment) and the neutral (normal cells).

To identify if the drug molecules of DOX and photoactive DPP have been loaded on $MgSiO_3$:Eu DCMPs, we measured the FT-IR spectra of DCMPs, DCMPs-NH_2, DCMPs-NH_2-DOX, and DCMPs-NH2-DOX-DPP (Fig. S3), and the FT-IR spectrum of as-synthesized DPP is also presented in Fig. S4. It can be seen that DOX can be conjugated after DCMPs was modified with -NH_2 groups. And with the assistance of EDC/NHS, DPP with -COOH bands can also be conjugated onto the surface of the sample. To determine the actual loading amount of DPP, the supernatants of the solutions after DPP was loaded were collected for ICP-MS measurement. After calculation, the exact loading amount of DPP on DCMPs-NH_2-DOX is 1.13 mg when the added amount is 3.0 mg.

Meanwhile, DPP has no obvious absorbance in visible region, and it is sensitive to UV light which overlaps with the excitation wavelength. To make clear the role of UV light, DCMPs-DPP without loaded DOX was prepared. Fig. S5A shows the release properties of Pt from the DCMPs carrier under different pH values (5.5 and 7.0), and the efficiencies have little difference under acid and neutral environment, which indicates the acid may have no obvious influence on photoactivated DPP prodrugs.[53] Differently, Fig. S5B shows the release properties with and without UV light irradiation (pH = 5.5), indicating the UV light can promote the release of Pt from DCMPs. The postulated drug release pathway of photoactive DPP to Pt(II) drugs is proposed in Fig. S5C. Under the aqueous environment, the UV light could not only break Pt-N bonds but also activate the DPP to translate Pt(IV) to Pt(II). Finally, Pt(II) molecules can play a role as the anti-cancer drugs.

In order to make the treatment condition be concordant, UV irradiation with the pump power of 0.2 W cm^{-2} for 30 min was carried out in the three groups. In Fig. 9D, the viability of HeLa cells incubated with pure DOX with different concentrations is 42.1%-76.3%, and the corresponding IC_{50} value of this treatment is 20.0 μg mL^{-1}. When the $MgSiO_3$:Eu is used as the drug carrier, the viability of HeLa cells incubated with $MgSiO_3$:Eu-DOX-RGD is 38.2%-67.2%, and the IC_{50} value is 2.3 μg mL^{-1}. It is obvious that this group has higher toxicity to cells

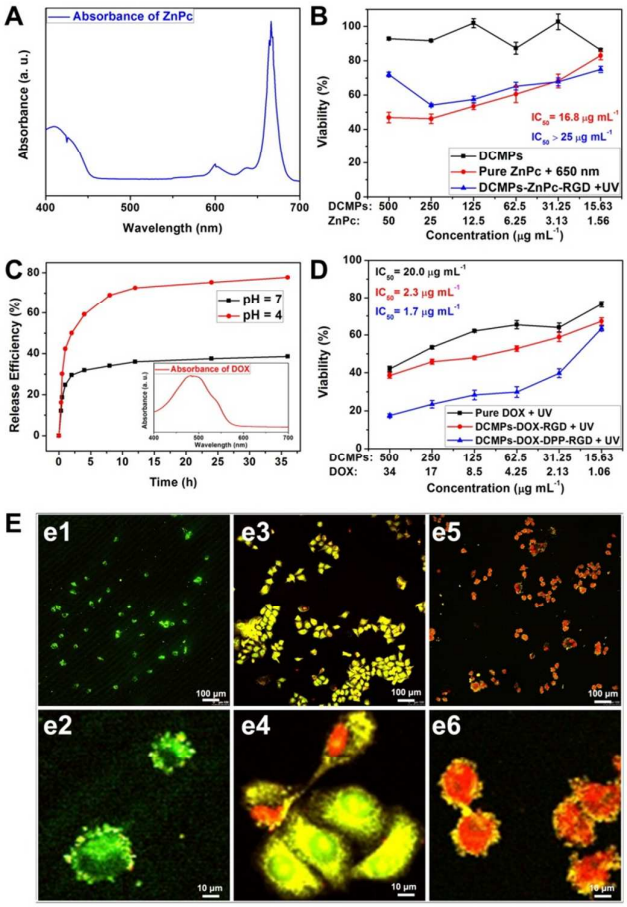

Fig. 9 (A) UV-vis absorbance spectrum of pure ZnPc solution. (B) Cell viability of HeLa cells incubated with pure DMCPs, pure ZnPc under 650 nm irradiation, and DCMPs-RGD-ZnPc under UV irradiation using MTT assay. (C) The release efficiency of DOX from DMCPs at different pH values. Inset is the UV-vis absorbance spectrum of pure DOX solution. (D) Cell viability of HeLa cells incubated with pure DOX, DCMPs-DOX-RGD, and DCMPs-DOX-DPP-RGD under UV irradiation using MTT assay. All the three groups are exposed under UV irradiation for 30 min with pump power of 0.2 W/cm^2. (E) CLSM images with different magnification of HeLa cells incubated with DCMPs for 60 min (e1, e2), with DCMPs-DOX-DPP-RGD for 60 min (e3, e4), with DCMPs-DOX-DPP-RGD under UV irradiation for 8 h (e5, e6). All the cells were dyed with calcein AM and PI.

due to the endocytosis process instead of passive diffusion, which results in the fast and efficient accumulation of drug in the cytoplasm. The fast release and the following controlled modest release of DOX due to the mesoporous channels and cavities promote the final high anti-cancer therapy efficacy. For even better anti-cancer therapy, DPP pro-drugs which could be changed into toxic cisplatin under UV irradiation were further conjugated onto the carriers. As depicted, the viability of cells incubated with $MgSiO_3$:Eu-DOX-DPP-RGD under UV irradiation is lower than the former two groups with the highest value of 17.4% (with the highest concentration of 1 mg mL^{-1}). The IC_{50} value of this treatment is low as 1.7 μg mL^{-1}. That means, this $MgSiO_3$:Eu-DOX-DPP-RGD platform with imaging property under UV irradiation has excellent anti-cancer therapeutic efficacy *in vitro*.

Although MTT assay is essential and important, sometimes it is not very accurate due to the chromophore disturbance of different drug molecules (DOX and ZnPc, *et al.*). Then, we used the live/dead state of tumor cells to further evaluate the cytotoxicity of the carrier with loaded drug molecules. CLSM images of HeLa cells dyed with calcein AM and PI after different treatments are presented in Fig. 9E. CLSM images of HeLa cells incubated with pure $MgSiO_3$:Eu for 60 min are given in Fig. 9e1, e2. As depicted, the cells present strong green signals in the whole cells which indicate the material is nontoxic. Meanwhile, there are yellow and red signals in the cytoplasm and cell membrane, which indicates part of $MgSiO_3$:Eu spheres is intracellular. When HeLa cells were incubated with $MgSiO_3$:Eu-DOX-DPP-RGD for 60 min without UV irradiation, several cells are killed with the nuclei dyed with red emission (Fig. 9e3, e4). Importantly, compared with HeLa cells incubated with pure $MgSiO_3$:Eu, HeLa cells incubated with $MgSiO_3$:Eu-DOX-DPP-RGD for the same time have higher yellow and red signals in the cytoplasm which further proves the targeted effect of RGD. This result is also consistent with the result as depicted in Fig. 5. Note that only DOX in the platform plays the anti-cancer role to kill cells, and photo-activated DPP molecules have no obvious toxicity to cancer cells without UV irradiation. Thus, many cells still live due to the short chemotherapeutic time. As discussed in the MTT assay, the $MgSiO_3$:Eu-DOX-DPP-RGD could be cytotoxic to cancer cells after 24 h incubation, because DOX plays a key role with long incubation time. Consequently, when HeLa cells are incubated with $MgSiO_3$:Eu-DOX-DPP-RGD for 8 h with UV irradiation, almost all of the HeLa cells are killed (Fig. 9e5,9e6). In Fig. 9e6, the nuclei are dyed to red with residual yellow signals in the cytoplasm.

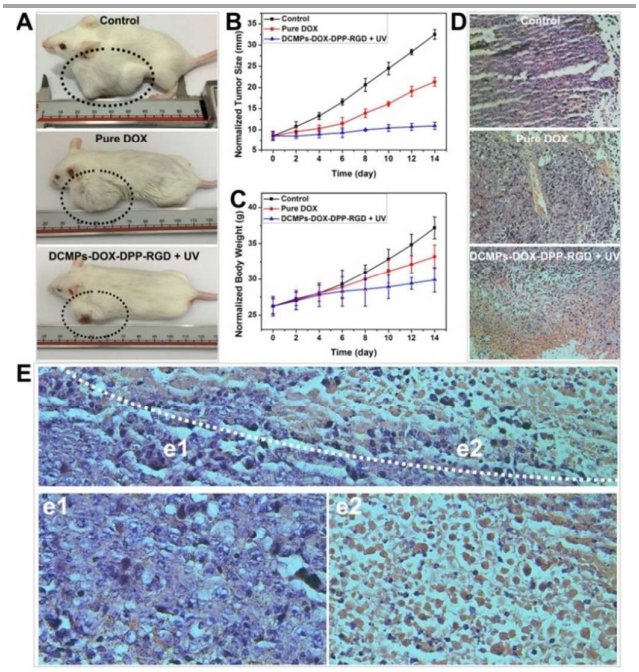

Fig. 10 (A) Photographs of tumor-bearing mice after different treatments: without treatment (control), with DOX, with DCMPs-DOX-DPP-RGD under UV irradiation. (B) The normalized tumor sizes and (C) body weights of mice after different treatments. (D) H&E stained images of tumor tissues from the corresponding groups obtained after 14 days treatment. (E) H&E stained images of tumor tissues from DCMPs-DOX-DPP-RGD under UV irradiation group after 7 days treatment.

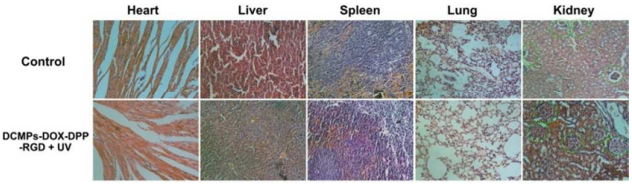

Fig. 11. H&E stained images of organ tissues from the control group and the best treated group of DCMPs-DOX-DPP-RGD under UV irradiation after 14 days treatment.

The anti-cancer therapeutic effect *in vivo* was further detected stimulated by the good biocompatibility and high anti-cancer efficacy *in vitro*. Three groups with different treatments were separately carried out. After treatment for 2 weeks, mice from different groups are presented in Fig. 10A. The average tumor size of mice in different groups is 32.5 mm, 21.3 mm, and 8.9 mm, respectively. It is obvious that the treatment in the third group has the highest inhibition efficacy to tumor sizes (Fig. 10B). Fig. 10C indicates the body weight in the third group keeps enhanced which indicates there is no abnormal state, and the enhanced weight in control group is attributed to the unlimited enhanced tumors. Additionally, the histological analysis of the tumor tissues (Fig. 10D) after treatment of $MgSiO_3$:Eu-DOX-DPP-RGD under UV irradiation for 14 days indicates the tumors are almost killed with a large amount of tumor apoptosis in this group compared with the first and second groups. The H&E stained images of tumor tissues taken from the third group at the 7^{th} treatment day are presented in Fig. 10E, there is an obvious layer between the necrotic cells and tumor cells. Compared with Fig. 10e1, Fig. 10e2 presents amount of pink dead cells with concentration of nuclei, indicating apoptosis appears in most of tumor cells. The histological analysis of the typical heart, lung, kidney, liver, and spleen of the mice is given in Fig. 11. There is a little glomerulus atrophy in the control group due to the unlimited and transferred tumor cells. Compared with the control group, there is no necrosis in any analysed histological tissues in the third group, hepatocytes in the liver samples are found normal, and there is no pulmonary fibrosis in the lung samples. Meanwhile, the glomerulus structure in the kidney section is clearly observed and there is no concentration tendency. The result indicates the third treatment ($MgSiO_3$:Eu-DOX-DPP-RGD with UV irradiation) could inhibit the tumors in a large extent, which is potential in clinical application.

Conclusions

In summary, we synthesized uniform $MgSiO_3$:Eu hollow microspheres through a sacrificed template method based on Kirkendall effect, which was used for anti-tumor carrier. The photoluminescence properties were detected and optimized for better bio-imaging, and the material could emit recognized red signal *in vitro* and *in vivo* under modest UV irradiation.

$MgSiO_3$:5%Eu DCMPs as the final drug carrier were used for loading chemotherapeutics drug of DOX and light-activated platinum(IV) prodrug of DPP. With the assistance of the targeted peptide of RGD, the platform could be intracellular through fast and effective endocytosis. Under UV irradiation, the platform exhibits high anti-cancer efficacy (only 17.4% of HeLa cancer cells survived) due to the release of dual drugs and targeting effect. *In vivo* results reveal that the group treated with $MgSiO_3$:Eu-DOX-DPP-RGD injection under UV irradiation could markedly inhibit the growth of tumor. Owing to the good bioimaging property and high anti-cancer efficacy, this functional platform should be high promising in imaging-guided anti-cancer therapy field.

Acknowledgements

Financial supports from the National Natural Science Foundation of China (NSFC 21271053, 21401032, and 51472058), NCET in University (NCET-12-0622), Natural Science Foundation of Heilongjiang Province (B201403), Harbin Sci.-Tech. Innovation Foundation (2014RFQXJ019), Heilongjiang Postdoctoral Fund (LBH-Z14052), General Financial Grant from the China Postdoctoral Science Foundation (2014M560248) and Fundamental Research Funds for the Central Universities of China are greatly acknowledged.

Notes and references

1 S. Gai, C. Li, P. Yang and J. Lin, *Chem. Rev.*, 2013, **114**, 2343-2389.
2 Y. H. Bae and K. Park, *J. Control. Release*, 2011, **153**, 198-205.
3 G. Tian, X. Zheng, X. Zhang, W. Yin, J. Yu, D. Wang, Z. Zhang, X. Yang, Z. Gu and Y. Zhao, *Biomaterials*, 2015, **40**, 107-116.
4 C. E. Ashley, E. C. Carnes, G. K. Phillips, D. Padilla, P. N. Durfee, P. A. Brown, T. N. Hanna, J. Liu, B. Phillips, M. B. Carter, N. J. Carroll, X. Jiang, D. R. Dunphy, C. L. Willman, D. N. Petsev, D. G. Evans, A. N. Parikh, B. Chackerian, W. Wharton, D. S. Peabody and C. J. Brinker, *Nat. Mater.,* 2011, **10**, 389-397.
5 J. Yang, W. Liu, M. Sui, J. Tang and Y. Shen, *Biomaterials*, 2011, **32**, 9136-9143.
6 X. Liu, F. Fu, K. Xu, R. Zou, J. Yang, Q. Wang, Q. Liu, Z. Xiao and J. Hu, *J. Mater. Chem. B,* 2014, **2**, 5358-5367.
7 J. Kim, H. S. Kim, N. Lee, T. Kim, H. Kim, T. Yu, I. C. Song, W. K. Moon and T. Hyeon, *Angew. Chem. Int. Ed.,* 2008, **47**, 8438-8441.
8 Y. Liu, Y. Liu, W. Bu, Q. Xiao, Y. Sun, K. Zhao, W. Fan, J. Liu and J. Shi, *Biomaterials*, 2015, **49**, 1-8.
9 H. S. Qian, H. C. Guo, P. C.-L. Ho, R. Mahendran and Y. Zhang, *Small*, 2009, **5**, 2285-2290.
10 L. Yu, H. B. Wu and X. W. Lou, *Adv. Mater.*, 2013, **25**, 2296-2300.
11 Z. Li and Y. Zhang*, Angew. Chem. Int. Ed.,* 2006, **45**, 7732-7735.
12 T. Kim, E. Momin, J. Choi, K. Yuan, H. Zaidi, J. Kim, M. Park, N. Lee, M. T. McMahon, A. Quinones-Hinojosa, J. W. M. Bulte, T. Hyeon and A. A. Gilad, *J. Am. Chem. Soc.*, 2011, **133**, 2955-2961.
13 Y. Chen, Q. Meng, M. Wu, S. Wang, P. Xu, H. Chen, Y. Li, L. Zhang, L. Wang and J. Shi, *J. Am. Chem. Soc.*, 2014, **136**, 16326-16334.
14 14.H. M. Chen, R.-S. Liu, M.-Y. Lo, S.-C. Chang, L.-D. Tsai, Y.-M. Peng and J.-F. Lee, *J. Phys. Chem. C,* 2008, **112**, 7522-7526.
15 X. Yang, J. Fu, C. Jin, J. Chen, C. Liang, M. Wu and W. Zhou, *J. Am. Chem. Soc.*, 2010, **132**, 14279-14287.
16 B. Liu, Q. Wang, S. Yu, T. Zhao, J. Han, P. Jing, W. Hu, L. Liu, J. Zhang, L.-D. Sun and C.-H. Yan, *Nanoscale*, 2013, **5**, 9747-9757.
17 W. Fang, S. Tang, P. Liu, X. Fang, J. Gong and N. Zheng, *Small*, 2012, **8**, 3816-3822.
18 B. Wang, H. B. Wu, L. Zhang and X. W. Lou, *Angew. Chem. Int. Ed. Engl.*, 2013, **52**, 4165-4168.
19 X. Liu, C.-H. Yan and J. A. Capobianco, *Chem. Soc. Rev.*, 2015, **44**, 1299-1301.
20 Y. Yang, Q. Shao, R. Deng, C. Wang, X. Teng, K. Cheng, Z. Cheng, L. Huang, Z. Liu, X. Liu and B. Xing, *Angew. Chem. Int. Ed.,* 2012, **51**, 3125-3129.
21 M. K. G. Jayakumar, A. Bansal, K. Huang, R. Yao, B. N. Li and Y. Zhang, *Acs Nano*, 2014, **8**, 4848-4858.
22 T. Maldiney, A. Bessiere, J. Seguin, E. Teston, S. K. Sharma, B. Viana, A. J. J. Bos, P. Dorenbos, M. Bessodes, D. Gourier, D. Scherman and C. Richard, *Nat. Mater.,* 2014, **13**, 418-426.
23 C. P. Montgomery, B. S. Murray, E. J. New, R. Pal and D. Parker, *Acc. Chem. Res.*, 2009, **42**, 925-937.
24 X. Song, H. Gong, T. Liu, L. Cheng, C. Wang, X. Sun, C. Liang and Z. Liu, *Small*, 2014, **10**, 4362-4370.
25 G. Chen, J.-Y. Zhu, Z.-L. Zhang, W. Zhang, J.-G. Ren, M. Wu, Z.-Y. Hong, C. Lv, D.-W. Pang and Y.-F. Zhao, *Angew. Chem. Int. Ed.,* 2015, **54**, 1036-1040.
26 W. Sun, J. Yu, R. Deng, Y. Rong, B. Fujimoto, C. Wu, H. Zhang and D. T. Chiu, *Angew. Chem. Int. Ed.,* 2013, **52**, 11294-11297.
27 D. Ananias, F. A. Almeida Paz, D. S. Yufit, L. D. Carlos and J. Rocha, *J. Am. Chem. Soc.*, 2015, **137**, 3051-3058.
28 C. Wang, L. Cheng, Y. Liu, X. Wang, X. Ma, Z. Deng, Y. Li and Z. Liu, *Adv. Funct. Mater.*, 2013, **23**, 3077-3086.
29 X. Teng, Y. Zhu, W. Wei, S. Wang, J. Huang, R. Naccache, W. Hu, A. I. Y. Tok, Y. Han, Q. Zhang, Q. Fan, W. Huang, J. A. Capobianco and L. Huang, *J. Am. Chem. Soc.*, 2012, **134**, 8340-8343.
30 W. Zheng, P. Huang, D. Tu, E. Ma, H. Zhu and X. Chen, *Chem. Soc. Rev.*, 2015, **44**, 1379-1415.
31 D. J. Gargas, E. M. Chan, A. D. Ostrowski, S. Aloni, M. V. P. Altoe, E. S. Barnard, B. Sanii, J. J. Urban, D. J. Milliron, B. E. Cohen and P. J. Schuck, *Nat. Nanotechn.*, 2014, **9**, 300-305.
32 A. Hlavacek, A. Sedlmeier, P. Skladal and H. H. Gorris, *ACS Appl. Mater. Inter.,* 2014, **6**, 6930-6935.
33 Y. Wu, Y. Sun, X. Zhu, Q. Liu, T. Cao, J. Peng, Y. Yang, W. Feng and F. Li, Biomaterials, 2014, **35**, 4699-4705.
34 Y. Zhou and B. Yan, *Nanoscale*, 2015, **7**, 4063-4069.
35 P. Li, Q. Peng and Y. Li, *Adv. Mater.*, 2009, **21**, 1945-1948.
36 L. Raehm, A. Mehdi, C. Wickleder, C. Reyé and R. J. P. Corriu, *J. Am. Chem. Soc.*, 2007, **129**, 12636-12637.
37 K. Kompe, H. Borchert, J. Storz, A. Lobo, S. Adam, T. Moller and M. Haase, *Angew. Chem. Inter. Ed.*, 2003, **42**, 5513-5516.
38 D. Tu, L. Liu, Q. Ju, Y. Liu, H. Zhu, R. Li and X. Chen, *Angew. Chem. Int. Ed.*, 2011, 50, 6306-6310.
39 J.-C. G. Buenzli, *Chem. Rev.*, 2010, **110**, 2729-2755.
40 S. S. Agasti, A. Chompoosor, C.-C. You, P. Ghosh, C. K. Kim and V. M. Rotello, *J. Am. Chem.* Soc., 2009, **131**, 5728-5729.
41 S. Angelos, Y.-W. Yang, N. M. Khashab, J. F. Stoddart and J. I. Zink, *J. Am. Chem. Soc.*, 2009, **131**, 11344-11346.
42 E. Aznar, M. Dolores Marcos, R. Martinez-Manez, F. Sancenon, J. Soto, P. Amoros and C. Guillem, *J. Am. Chem. Soc.*, 2009, **131**, 6833-6843.
43 H.-C. Joo, Y.-J. Lim, M.-J. Kim, H.-B. Kwon and J.-H. Han, *Appl. Surf. Sci.*, 2010, **257**, 741-746.

44 F. Meiser, C. Cortez and F. Caruso, *Angew. Chem. Int. Ed.,* 2004, **43**, 5954-5957.
45 K. P. F. Siqueira, P. P. Lima, R. A. S. Ferreira, L. D. Carlos, E. M. Bittar, E. Granado, J. C. Gonzalez, A. Abelenda, R. L. Moreira and A. Dias, Chem. Mater., 2014, **26**, 6351-6360.
46 S. Zeng, H. Wang, W. Lu, Z. Yi, L. Rao, H. Liu and J. Hao, *Biomaterials*, 2014, **35**, 2934-2941.
47 B. Voss, J. Nordmann, A. Uhl, R. Komban and M. Haase, *Nanoscale*, 2013, **5**, 806-812.
48 W. Lu, N. Guo, Y. Jia, Q. Zhao, W. Lv, M. Jiao, B. Shao and H. You, *Inorg. Chem.*, 2013, **52**, 3007-3012.
49 B. Shao, Q. Zhao, N. Guo, Y. Jia, W. Lv, M. Jiao, W. Lu and H. You, *Cryst. Growth Des.,* 2013, **13**, 3582-3587.
50 R. Lv, G. Yang, S. Gai, Y. Dai, F. He and P. Yang, *RSC Adv.*, 2014, **4**, 63425-63435.
51 O. Lehmann, K. Kompe and M. Haase, *J. Am. Chem. Soc.*, 2004, **126**, 14935-14942.
52 X. He and B. Yan, *J. Mater. Chem. C,* 2013, **1**, 3910-3912.
53 Y. Dai, H. Xiao, J. Liu, Q. Yuan, P. a. Ma, D. Yang, C. Li, Z. Cheng, Z. Hou, P. Yang and J. Lin, *J. Am. Chem. Soc.*, 2013, **135**, 18920-18929.
54 R. Lv, S. Gai, Y. Dai, F. He, N. Niu and P. Yang, *Inorg. Chem.*, 2014, 53, 998-1008.
55 C. C. Lin, Z. R. Xiao, G.-Y. Guo, T.-S. Chan and R.-S. Liu, *J. Am. Chem. Soc.*, 2010, **132**, 3020-3028.
56 V. T. Freitas, L. Fu, A. M. Cojocariu, X. Cattoen, J. R. Bartlett, R. Le Parc, J.-L. Bantignies, M. Wong Chi Man, P. S. Andre, R. A. S. Ferreira and L. D. Carlos, *ACS Appl. Mater. Inter.,* 2015, **7**, 8770-8778.
57 Y. Zhang, D. L. Geng, X. J. Kang, M. M. Shang, Y. Wu, X. J. Li, H. Z. Lian, Z. Y. Cheng and J. Lin, *Inorg. Chem.*, 2013, **52**, 12986-12994.

$MgSiO_3$:Eu-DOX-DPP-RGD hollow microspheres employed for simultaneous imaging and anti-cancer therapy has been designed by sequentially loading DOX, DPP, and targeted peptide of RGD on $MgSiO_3$:Eu hollow spheres.